

Double exchange in a magnetically frustrated system

R S Fishman

Condensed Matter Sciences Division, Oak Ridge National Laboratory, Oak Ridge,
TN 37831-6032, USA

Received 12 April 2004

Published 16 July 2004

Online at stacks.iop.org/JPhysCM/16/5483

doi:10.1088/0953-8984/16/30/011

Abstract

This work examines the magnetic order and spin dynamics of a double-exchange model with competing ferromagnetic and antiferromagnetic Heisenberg interactions between the local moments. The Heisenberg interactions are periodically arranged in a Villain configuration in two dimensions with nearest-neighbour, ferromagnetic coupling J and antiferromagnetic coupling $-\eta J$. This model is solved at zero temperature by performing a $1/\sqrt{S}$ expansion in the rotated reference frame of each local moment. When η exceeds a critical value, the ground state is a magnetically frustrated, canted antiferromagnet. With increasing hopping energy t or magnetic field B , the local moments become aligned and the ferromagnetic phase is stabilized above critical values of t or B . In the canted phase, a charge-density wave forms because the electrons prefer to sit on lines of sites that are coupled ferromagnetically. Due to a change in the topology of the Fermi surface from closed to open, phase separation occurs in a narrow range of parameters in the canted phase. In zero field, the long-wavelength spin waves are isotropic in the region of phase separation. Whereas the average spin-wave stiffness in the canted phase increases with t or η , it exhibits a more complicated dependence on field. This work strongly suggests that the jump in the spin-wave stiffness observed in $\text{Pr}_{1-x}\text{Ca}_x\text{MnO}_3$ with $0.3 \leq x \leq 0.4$ at a field of 3 T is caused by the delocalization of the electrons rather than by the alignment of the antiferromagnetic regions.

1. Introduction

The persistence of antiferromagnetic (AFM) short-range order in the ferromagnetic (FM) phase of the manganites has been recognized for many years [1]. In metallic manganites like $\text{La}_{0.7}\text{Ca}_{0.3}\text{MnO}_3$ that contain a preponderance of AFM-coupled polaronic regions [2, 3], the Curie temperature T_C is suppressed but the magnetoresistance is strongly enhanced. Close to but below T_C , the spin dynamics of $\text{La}_{0.7}\text{Ca}_{0.3}\text{MnO}_3$ contains both a propagating spin-wave (SW) branch from the FM regions and a diffusive component from polaronic regions with suppressed FM interactions [4]. The low-temperature insulating phase of the manganite $\text{Pr}_{1-x}\text{Ca}_x\text{MnO}_3$ with $0.3 \leq x \leq 0.4$ was originally believed [5–7] to be a canted AFM (CAF)

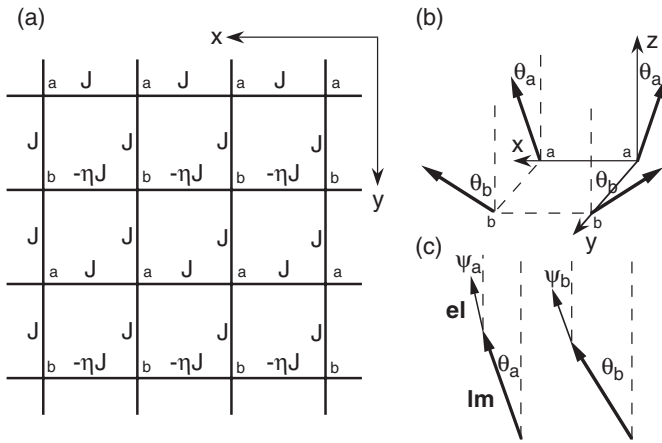


Figure 1. (a) The generalized Villain model with Heisenberg couplings J or $-\eta J$, (b) the local moments in the xz plane subtend angles θ_a and θ_b with the z axis, and (c) the electron spins also lie in the xz plane but subtend angles $\psi_a < \theta_a$ and $\psi_b < \theta_b$ with the z axis.

but may actually contain regions with both FM and AFM short-range order [8–13]. When an applied field B exceeds about 3 T, the resistivity drops by several orders of magnitude [6], the AFM regions shrink [12], and the SW stiffness D_{sw} jumps by a factor of three [11]. Despite the central role played by AFM interactions in the manganites, little is known theoretically about how they affect the propagating SW dynamics. As first shown by Anderson and Hasegawa [14], the effective electron-hopping energy between two local moments making a relative angle Θ is proportional to $\cos \Theta/2$ in the limit of large Hund's coupling. So AFM interactions may suppress the contribution of electron-mediated double-exchange (DE) to the SW dynamics [15]. By aligning the local moments, a magnetic field or electron hopping will alter the DE contribution to the SW dynamics. This paper examines the effects of AFM interactions on the ground-state properties and SW dynamics of electrons coupled to the local moments of a generalized Villain model [16–19].

The generalized Villain model is one of the simplest periodic models to exhibit magnetic frustration. As described in figure 1(a), three-dimensional local moments \mathbf{S}_i are coupled by the FM interaction J along the y direction and by either the FM interaction J or the AFM interaction $-\eta J$ along the x direction. The CAF phase is stable when η exceeds the critical value η_c , which is $1/3$ when $\mathbf{B} = B\hat{z} = 0$ but increases as B increases. Due to the different environments of the a and b sites, the angle θ_b at the b sites is always larger than θ_a at the a sites, as shown in figure 1(b).

In the hybrid model considered here, the Heisenberg interactions between the local moments are in the Villain configuration while electrons with density $p = 1 - x$ are FM coupled to the local moments by Hund's coupling J_H and hop between neighbouring sites with energy t . The DEV model (so called because it combines the DE and Villain models) provides several advantages as a basis for understanding the effects of AFM interactions and non-collinearity on the spin dynamics. First, except in a narrow range of parameters, a homogeneous CAF phase is stable against phase separation when the AFM control parameter η exceeds η_c . By contrast, the well-studied hybrid model with AFM interactions $-J$ between all neighbouring local moments phase separates *before* the AFM exchange J is large enough to cant the spins [20–23]. This phase instability is caused by a ‘site-local continuous degeneracy’ [21, 23]¹ that is absent in

¹ In the canted phase of a two-sublattice model with AFM interactions, the local moment on any site of sublattice a must make an angle Θ with the local moments on sublattice b . So the possible orientations for any a spin trace out a cone around the equilibrium direction of the b spins [21, 23]. In the canted phase of a two-sublattice model with FM interactions in plane but AFM interactions between planes, the moments in any plane a are free to rotate about the equilibrium direction of the moments on neighbouring planes b . These local or planar degeneracies are absent in the DEV model.

the DEV model. Second, unlike the case in a hybrid model with AFM exchange only, the ground state of the DEV model contains a FM component even when $t = 0$ and $B = 0$. So it can be used to evaluate the change in SW stiffness D_{sw} as the electrons become mobile. Third, because the DEV model contains both FM and AFM Heisenberg interactions, it can be used to study insulating manganites like $\text{Pr}_{0.66}\text{Ca}_{0.34}\text{MnO}_3$, where the AFM interactions are produced by superexchange and the FM interactions by short-ranged orbital order [24]².

For simplicity, we have constructed a model that is translationally symmetric in two dimensions. Since this model is solved at zero temperature, the qualitative results will be unchanged in three dimensions. More problematically, the AFM interactions are arranged periodically rather than in clusters. In the low-temperature phase of $\text{Pr}_{0.67}\text{Ca}_{0.33}\text{MnO}_3$, the FM interactions may be confined to two-dimensional sheets with widths of roughly 25 Å in a ‘red cabbage’ structure [12, 13]. Neutron-scattering results [11], on the other hand, suggest that the FM clusters in the insulating phase are about 40 Å in diameter. So for wavelengths much longer than 40 Å, the SWs will average over the FM and AFM regions. Hence, the DEV model will provide qualitatively accurate predictions for the average SW stiffness $D_{\text{sw}}^{\text{av}} = (D_{\text{sw}}^x + D_{\text{sw}}^y)/2$ defined in the long-wavelength limit.

The Hamiltonian of the DEV model is given by

$$H = -t \sum_{\langle i,j \rangle} \sum_{\alpha} (c_{i\alpha}^{\dagger} c_{j\alpha} + c_{j\alpha}^{\dagger} c_{i\alpha}) - 2J_{\text{H}} \sum_i \mathbf{s}_i \cdot \mathbf{S}_i - \sum_{\langle i,j \rangle} J_{ij} \mathbf{S}_i \cdot \mathbf{S}_j - B \sum_i S_{iz}, \quad (1)$$

where $c_{i\alpha}^{\dagger}$ and $c_{i\alpha}$ are the creation and destruction operators for an electron with spin α at site i , $\mathbf{s}_i = (1/2)c_{i\alpha}^{\dagger} \boldsymbol{\sigma}_{\alpha\beta} c_{i\beta}$ is the electronic spin, and \mathbf{S}_i is the spin of the local moment with magnitude S . Nearest-neighbour Heisenberg interactions J_{ij} take the values J (FM interaction) or $-\eta J$ (AFM interaction), as described in figure 1(a). This model is solved at zero temperature by expanding the Hamiltonian in powers of $1/\sqrt{S}$. To guarantee that the contributions to the SW frequencies from hopping and from the Heisenberg interactions are of the same order in $1/\sqrt{S}$, t is considered to be of the same order in $1/\sqrt{S}$ as $J_{\text{H}}S$, $J S^2$ and $B S$. Hence, the dimensionless parameters of our model are $t' = t/J S^2$, η , $B' = B/J S$ and $J_{\text{H}}/J S$. To lowest order in $1/S$, the magnetic field B only couples to the local moments and not to the electrons. While the theory developed below can be extended to treat all values of the Hund’s coupling, we shall for simplicity consider the limit of large $J_{\text{H}}S$ or in dimensionless terms, $J_{\text{H}}/J S \gg 1$ and $J_{\text{H}}S/t \gg 1$. An earlier work [25] discussed the dependence of the SW dynamics on t' . Those results are substantially extended here to describe the dependence on η and field.

This paper is divided into five sections. The Villain model is discussed in some detail in section 2, where we provide new results for the SW stiffness. The ground-state properties of the DEV model are presented in section 3. In section 4, we evaluate the SW frequencies of the DEV model. Section 5 contains a discussion and summary. Two appendices contain results for the coefficients of the harmonic Hamiltonian and for the hopping matrix elements of the band Hamiltonian.

2. Generalized Villain model

This section presents, for the first time, a Holstein–Primakoff expansion for the generalized Villain model. In an equivalent approach, Saslow and Erwin [19] numerically evaluated the mode frequencies by linearizing the equations of motion for the spins. However, a formal

² While the FM coupling between neighbouring Mn^{4+} and Mn^{3+} ions are induced by the hopping of electrons between those sites, that coupling is significantly enhanced by the polaronic distortions of the O atoms around some Mn^{4+} ions [24]. So the Heisenberg coupling J incorporates the enhancement of the FM interaction beyond that produced by the uniform hopping of electrons between neighbouring sites on an undistorted lattice.

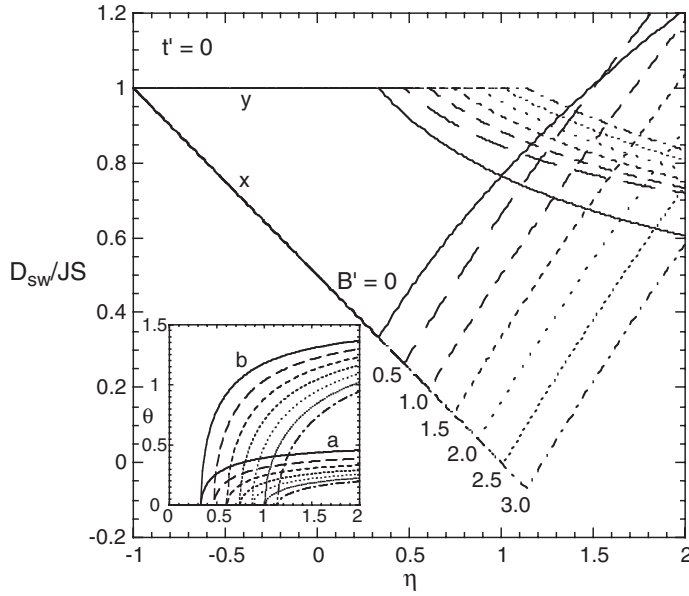


Figure 2. The SW stiffnesses versus η for $t' = 0$ and various values of the field B' . In the inset are plotted the equilibrium angles θ_a and θ_b versus η for the same set of fields.

Holstein–Primakoff expansion is required to lay the foundation for the solution of the full DEV model in section 4.

The Hamiltonian H_v of the generalized Villain model is given by equation (1) with $t = 0$ and $J_H = 0$. The spin dynamics is immensely simplified in the rotated reference frame for each spin: $\bar{\mathbf{S}}_i = \underline{U}_i^{\text{rot}} \mathbf{S}_i$, where $\underline{U}_i^{\text{rot}}$ is the unitary rotation matrix for site i . A Holstein–Primakoff expansion is performed within each rotated reference frame: $\bar{S}_{iz} = S - a_i^\dagger a_i$, $\bar{S}_{ix} + i\bar{S}_{iy} = \sqrt{2S}a_i$ and $\bar{S}_{ix} - i\bar{S}_{iy} = \sqrt{2S}a_i^\dagger$. Then the zeroth-order term (in powers of $1/\sqrt{S}$) in H_v can be written as

$$E_h = \frac{1}{2} N J S^2 \left\{ -\cos 2\theta_a + \eta \cos 2\theta_b - 2 \cos(\theta_a - \theta_b) - B' (\cos \theta_a + \cos \theta_b) \right\}, \quad (2)$$

which is of order $J S^2$.

Minimizing E_h with respect to θ_a and θ_b yields the relations

$$\sin 2\theta_a + \sin(\theta_a - \theta_b) + \frac{1}{2} B' \sin \theta_a = 0, \quad (3)$$

$$-\eta \sin 2\theta_b - \sin(\theta_a - \theta_b) + \frac{1}{2} B' \sin \theta_b = 0. \quad (4)$$

In zero field, it is easy to show that $\theta_b = 3\theta_a$ for all η . The equilibrium angles are plotted versus η for several different values of B' ranging from 0 to 3 in the inset to figure 2. In the limit of large η with $B' = 0$, $\theta_b \rightarrow \pi/2$ and $\theta_a \rightarrow \pi/6$. For nonzero field, θ_b still approaches $\pi/2$ but θ_a approaches an angle smaller than $\pi/6$. In figure 3(a), we plot the equilibrium angles versus B' for several values of η .

After linearizing equations (3) and (4), we find that the phase boundary between the CAF and FM phases satisfies the relation

$$B' - 2\eta + 4 - 2\sqrt{(\eta + 1)^2 + 1} = 0, \quad (5)$$

which was first obtained by Gabay *et al* [18]. While $\eta_c = 1/3$ in zero field, η_c increases with the field B' as seen in the inset to figure 2 and in 3(a).

Expanded as $H_v = E_h + H_{v1} + H_{v2} + \dots$ in powers of $1/\sqrt{S}$, the first-order term H_{v1} vanishes provided that the angles θ_a and θ_b satisfy equations (3) and (4). In terms of the

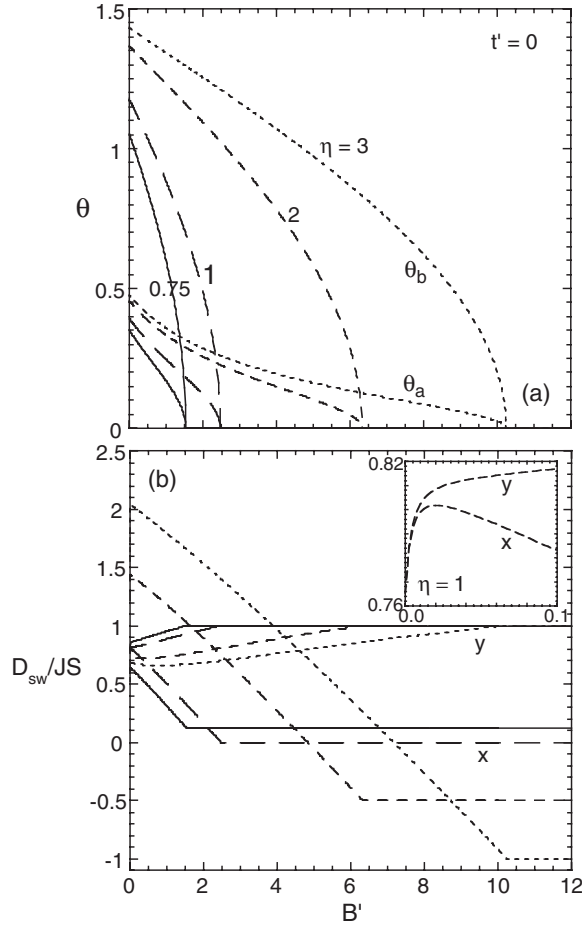


Figure 3. (a) Equilibrium angles and (b) SW stiffnesses versus applied field B' for several values of η and $t' = 0$. Inset in (b) are the SW stiffnesses when $\eta = 1$ for very small fields and $k_\alpha = 0.015\pi$.

Fourier-transformed spin operators $a_{\mathbf{k}}^{(r)}$ and $a_{\mathbf{k}}^{(r)\dagger}$ on the $r = a$ or b sublattice, the second-order term H_{v2} can be written as

$$H_{v2} = JS \sum_{\mathbf{k}, r, s} \{ a_{\mathbf{k}}^{(r)\dagger} a_{\mathbf{k}}^{(s)} A_{\mathbf{k}}^{(r,s)} + (a_{-\mathbf{k}}^{(r)} a_{\mathbf{k}}^{(s)} + a_{-\mathbf{k}}^{(r)\dagger} a_{\mathbf{k}}^{(s)\dagger}) B_{\mathbf{k}}^{(r,s)} \}, \quad (6)$$

with coefficients given in appendix A. The Hamiltonian of equation (6) is easily diagonalized by applying the method of Walker and Walstedt [26], which was originally developed for spin glasses. The SW frequency $\omega_{\mathbf{k}}$ is given by equation (A.10) of appendix A. This formal result agrees with the numerical results of Saslow and Erwin [19]. In the long-wavelength limit, the SW stiffnesses in the x and y directions are obtained from the expression $\lim_{\mathbf{k} \rightarrow 0} \omega_{\mathbf{k}} = B + D_{\text{sw}}^x k_x^2 + D_{\text{sw}}^y k_y^2$.

In the FM phase, the SW frequency can be solved analytically:

$$\omega_{\mathbf{k}} = B + JS(3 - \eta + (\eta - 1) \cos k_x) - JS \sqrt{(1 + \eta)^2 (1 - \cos k_x)^2 + 4 \cos^2 k_y}. \quad (7)$$

So for $k_x = 0$, $\omega_{\mathbf{k}} = B + 2JS(1 - \cos k_y)$ is independent of η . The SW stiffnesses in the FM phase are given by the simple results $D_{\text{sw}}^x = (JS/2)(1 - \eta)$ and $D_{\text{sw}}^y = JS$, independent of field. The FM phase becomes unstable when $\omega_{\mathbf{Q}} = 0$, where $\mathbf{Q} = (\pi, 0)$ is the AFM Bragg vector. This yields the same condition for the CAF-FM phase boundary as equation (5).

In the CAF phase, analytic results for the SW stiffnesses were found only when $B = 0$:

$$D_{\text{sw}}^x = \eta D_{\text{sw}}^y = JS\sqrt{2\eta}\sqrt{1 - \sqrt{\frac{\eta}{\eta+1}}}. \quad (8)$$

When $\eta \rightarrow \infty$, $D_{\text{sw}}^x \rightarrow JS\sqrt{2\eta}$ and $D_{\text{sw}}^y \rightarrow JS\sqrt{2/\eta}$. For $B > 0$, D_{sw}^y tends to a nonzero limit but D_{sw}^x still diverges as $\eta \rightarrow \infty$. So the average SW stiffness always diverges when $\eta \rightarrow \infty$, regardless of the field.

As shown in figure 2, D_{sw}^x is a linearly decreasing function of η in the FM phase below η_c . In the CAF phase above η_c , D_{sw}^x increases and D_{sw}^y decreases with η . Long-wavelength SWs become isotropic when D_{sw}^x and D_{sw}^y cross. For $B = 0$, $D_{\text{sw}}^x = D_{\text{sw}}^y$ when $\eta = 1$. This crossing point moves to progressively larger values of η with increasing field.

The SW stiffnesses are plotted versus field in figure 3(b) for four different values of η . In the FM phase above B_c , the stiffnesses are independent of field. But in the CAF phase below B_c , the dependence on field is more complex. For $\eta > 1$, $D_{\text{sw}}^x > D_{\text{sw}}^y$ at zero field and the stiffnesses cross as the field increases. If the SW stiffness in the α direction is defined at fixed k_α by $D_{\text{sw}}^\alpha(k_\alpha, B) = (\omega_{\mathbf{k}} - B)/k_\alpha^2$, then $D_{\text{sw}}^\alpha(k_\alpha, B)$ increases rapidly near the field $B^* = D_{\text{sw}}^\alpha(k_\alpha, 0)k_\alpha^2$ as shown in the inset to figure 3(b) for $k_\alpha = 0.015\pi$. As discussed in detail elsewhere [27], this behaviour is typical of any CAF with a quadratic SW dispersion. Since the drop in D_{sw}^x is then steeper than the rise in D_{sw}^y , $D_{\text{sw}}^{\text{av}}$ decreases with field for $B \gg B^*$.

Surprisingly, figure 3(b) indicates that the stiffness in the x direction becomes negative for sufficiently large η . To understand this behaviour, we have plotted the SW frequencies versus \mathbf{k} for $\eta = 1$ and several fields in figure 4(b). Due to the reduced symmetry of the CAF phase, the first Brillouin zone extends from $-\pi$ to π along k_x but from $-\pi/2$ to $\pi/2$ along k_y .³ Since $\omega_{\mathbf{Q}} = 0$ and $\omega_0 = B$ in the CAF phase, the SW stiffness in the x direction must decrease as the field B becomes comparable to JS . When $\eta = 1$, $D_{\text{sw}}^x = 0$ for all fields above $B_c = 2(\sqrt{5} - 1)JS \approx 2.472JS$. For $\eta > 1$ and $B > B_c$, $D_{\text{sw}}^x < 0$ in the FM phase.

The SW frequencies are plotted versus \mathbf{k} for $B = 0$ and various values of η in figure 4(a). When $\eta = -1$, all of the Heisenberg interactions equal J and the SWs are isotropic. For $\eta < \eta_c = 1/3$ in the FM phase, the SW frequencies are independent of η along k_y but not along k_x , as implied by equation (7). With increasing η in the CAF phase, the SW stiffness increases along the x direction but decreases along the y direction, as predicted by equations (8) and shown in figure 2. Also notice that the SW velocity at \mathbf{Q} is an increasing function of η in the CAF phase.

Both figures 4(a) and (b) indicate that the SW velocity at \mathbf{Q} softens as the CAF phase becomes unstable. In the FM phase, $d\omega_{\mathbf{k}}/dk_x$ vanishes at \mathbf{Q} for all $B > B_c$ or $\eta < \eta_c$. The softening of the SW velocity at the CAF–FM phase boundary is a very general result, as discussed by Román and Soto [28].

3. Ground-state properties of the DEV model

In this section, we discuss the ground-state properties of the DEV model, which is constructed by placing electrons with density p on the Villain lattice. An electron on site i is coupled to the local moment at that site by Hund's coupling $-2J_{\text{H}}\mathbf{s}_i \cdot \mathbf{S}_i$ and is allowed to hop to neighbouring sites with hopping energy t , as specified by the DEV Hamiltonian of equation (1).

³ Since there are four inequivalent sites on the Villain lattice, it might seem that the first Brillouin zone should be reduced in both the x and y directions. However, all a or b sites experience the same environment regardless of whether the spins tilt to the $+x$ or $-x$ directions: each a spin, for example, makes an angle of $\theta_b - \theta_a$ with its b neighbours and an angle $2\theta_a$ with its a neighbours.

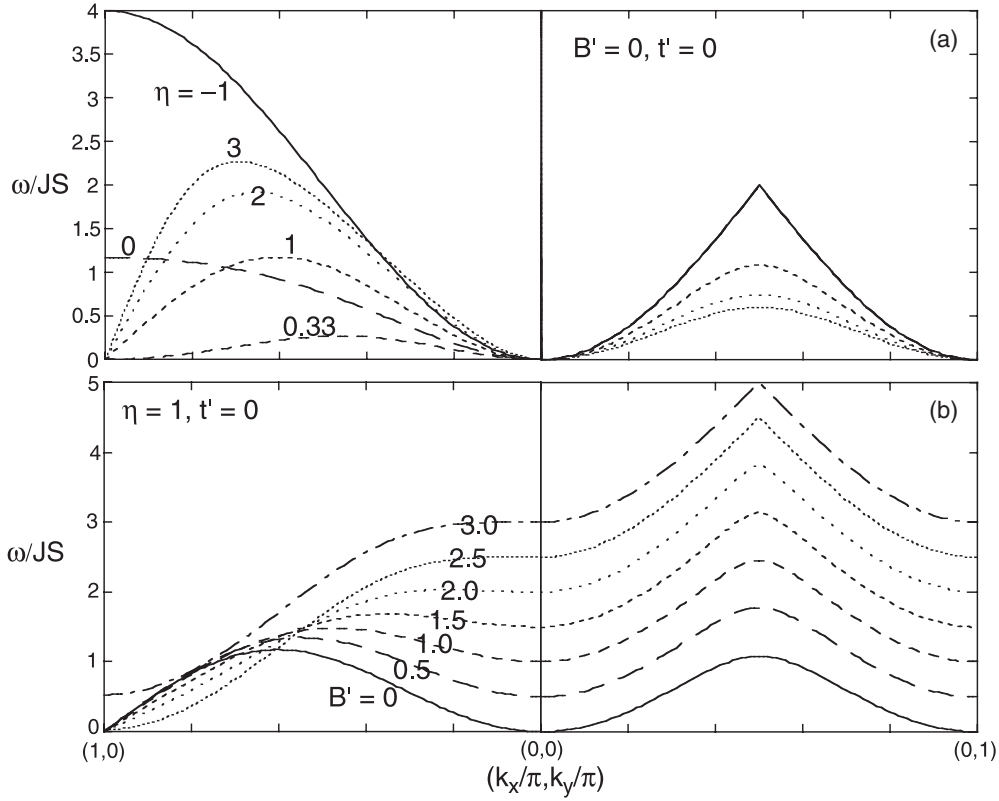


Figure 4. (a) The SW frequencies for $B' = 0, t' = 0$ and several values of η ; (b) the SW frequencies for $p = 0.66, \eta = 1, t' = 0$ and various fields B' .

With the Fermion creation and destruction operators $\bar{c}_{\mathbf{k}\alpha}^{(r)\dagger}$ and $\bar{c}_{\mathbf{k}\alpha}^{(r)}$ defined in the reference frames of the local moments, the band Hamiltonian of the electrons can be written

$$H_b = \sum_{\mathbf{k}} \sum_{i,j} \sum_{\alpha,\beta} (H_{b0\alpha\beta}^{ij} + K_{\alpha\beta}^{ij}(\mathbf{k})) \bar{c}_{\mathbf{k}\alpha}^{(i)\dagger} \bar{c}_{\mathbf{k}\beta}^{(j)}, \quad (9)$$

where $\bar{c}_{\mathbf{k}\alpha}^{(i)} = \{\bar{c}_{\mathbf{k}\alpha}^{(a)}, \bar{c}_{\mathbf{k}+\mathbf{Q},\alpha}^{(a)}, \bar{c}_{\mathbf{k}\alpha}^{(b)}, \bar{c}_{\mathbf{k}+\mathbf{Q},\alpha}^{(b)}\}$ defines the ij subspace. The sum over \mathbf{k} is restricted to the first Brillouin zone and $\alpha = \pm 1$ corresponds to spin up or down in the local reference frames. The zeroth-order band Hamiltonian includes just the Hund's coupling: $H_{b0\alpha\beta}^{ij} = -J_H S \delta_{ij} \sigma_{\alpha\beta}^z$. The hopping energies $K_{\alpha\beta}^{ij}(\mathbf{k})$, smaller by $t/J_H S$, are given in appendix B. Like E_h of equation (2), H_b is also of the order of $J S^2$.

The hopping energies $K_{\alpha\beta}^{ij}(\mathbf{k})$ are treated within degenerate perturbation theory. Second-order perturbation theory with corrections of order $t/J_H S$ will be required to obtain the SW frequencies in the next section. But to order $(t/J_H S)^0$ or to first order in the hopping energies, the spin up and down subspaces decouple and the band Hamiltonian H_b is easily transformed into the diagonal form $H_b = \sum_{\mathbf{k},\alpha,r} \epsilon_{\mathbf{k}\alpha}^{(r)} d_{\mathbf{k}\alpha}^{(r)\dagger} d_{\mathbf{k}\alpha}^{(r)}$ by the rotations $\bar{c}_{\mathbf{k}\alpha}^{(a)} = u_{\mathbf{k}}^{(a)} d_{\mathbf{k}\alpha}^{(a)} + u_{\mathbf{k}}^{(b)} d_{\mathbf{k}\alpha}^{(b)}$ and $\bar{c}_{\mathbf{k}\alpha}^{(b)} = u_{\mathbf{k}}^{(b)} d_{\mathbf{k}\alpha}^{(a)} - u_{\mathbf{k}}^{(a)} d_{\mathbf{k}\alpha}^{(b)}$ where $\epsilon_{\mathbf{k}\alpha}^{(r)} = -J_H S \alpha + \tilde{\epsilon}_{\mathbf{k}}^{(r)}$,

$$u_{\mathbf{k}}^{(a)2} = 1 - u_{\mathbf{k}}^{(b)2} = \frac{1}{2} \left\{ 1 + \frac{1}{w_{\mathbf{k}}} (\cos \theta_a - \cos \theta_b) \cos k_x \right\}, \quad (10)$$

$$\tilde{\epsilon}_{\mathbf{k}}^{(r)} = -t \cos k_x (\cos \theta_a + \cos \theta_b) \mp t w_{\mathbf{k}}, \quad (11)$$

$$w_{\mathbf{k}} = \sqrt{(\cos \theta_a - \cos \theta_b)^2 \cos^2 k_x + 4 \cos^2((\theta_a - \theta_b)/2) \cos^2 k_y}. \quad (12)$$

The upper and lower signs in $\tilde{\epsilon}_{\mathbf{k}}^{(r)}$ refer to the $r = a$ and b bands, respectively. With H_b in diagonal form, $E_b = \langle H_b \rangle$ is easy to evaluate.

It is straightforward to minimize the zeroth-order energy $E_0 = E_h + E_b$ with respect to the angles θ_a and θ_b in the limit of large $J_H S$. The relations that generalize equations (3) and (4) are

$$\sin 2\theta_a + \sin(\theta_a - \theta_b) + \frac{1}{2} B' \sin \theta_a + \frac{1}{NJS^2} \sum_{\mathbf{k}} \left\{ \frac{d\tilde{\epsilon}_{\mathbf{k}}^{(a)}}{d\theta_a} f(\tilde{\epsilon}_{\mathbf{k}}^{(a)}) + \frac{d\tilde{\epsilon}_{\mathbf{k}}^{(b)}}{d\theta_a} f(\tilde{\epsilon}_{\mathbf{k}}^{(b)}) \right\} = 0, \quad (13)$$

$$-\eta \sin 2\theta_b - \sin(\theta_a - \theta_b) + \frac{1}{2} B' \sin \theta_b + \frac{1}{NJS^2} \sum_{\mathbf{k}} \left\{ \frac{d\tilde{\epsilon}_{\mathbf{k}}^{(a)}}{d\theta_b} f(\tilde{\epsilon}_{\mathbf{k}}^{(a)}) + \frac{d\tilde{\epsilon}_{\mathbf{k}}^{(b)}}{d\theta_b} f(\tilde{\epsilon}_{\mathbf{k}}^{(b)}) \right\} = 0, \quad (14)$$

where $f(\tilde{\epsilon}) = \Theta(\tilde{\mu} - \tilde{\epsilon})$ is the Fermi function at $T = 0$ and $\tilde{\mu} = \mu - J_H S \operatorname{sgn}(p - 1)$ is the shifted chemical potential. For fixed η and B' , the equilibrium angles decrease with increasing t' . The phase boundary between the CAF and FM phases is now given by the condition

$$B' - 2\eta + 4 + 3K/4JS^2 - 2\sqrt{(1 + \eta)^2 + 1 + K/4JS^2 + (K/8JS^2)^2} = 0, \quad (15)$$

where $K = -(\langle \tilde{\epsilon}_{\mathbf{k}}^{(a)} \rangle + \langle \tilde{\epsilon}_{\mathbf{k}}^{(b)} \rangle)/2 \geq 0$ is the average kinetic energy of the electrons in the FM phase. This reduces to equation (5) when $K = 0$. For $t' = 10$ and $B' = 0$, the dependence of the equilibrium angles on η is plotted in figure 5(a). Also shown is the average spin $M = S(\cos \theta_a + \cos \theta_b)/2$ of the local moments. Their dependence on field B' is plotted in figure 6(a) for $t' = 3$ and $\eta = 2$. Both θ_a and θ_b were shown to vanish as $t' \rightarrow t'_c$ in [25].

Surprisingly, the electronic occupation of the a and b sites on the Villain lattice are different. For $p < 1$, the occupancies of the a and b sublattices are given by

$$n_a = \frac{2}{N} \sum_{\mathbf{k}} \left\{ u_{\mathbf{k}}^{(a)2} f(\tilde{\epsilon}_{\mathbf{k}}^{(a)}) + u_{\mathbf{k}}^{(b)2} f(\tilde{\epsilon}_{\mathbf{k}}^{(b)}) \right\}, \quad (16)$$

$$n_b = \frac{2}{N} \sum_{\mathbf{k}} \left\{ u_{\mathbf{k}}^{(b)2} f(\tilde{\epsilon}_{\mathbf{k}}^{(a)}) + u_{\mathbf{k}}^{(a)2} f(\tilde{\epsilon}_{\mathbf{k}}^{(b)}) \right\}. \quad (17)$$

From the relation $u_{\mathbf{k}}^{(a)2} + u_{\mathbf{k}}^{(b)2} = 1$, it follows that $(n_a + n_b)/2 = p$ is just the average number of electrons per site.

In the CAF phase, electrons prefer to sit on the a sites of the Villain lattice. The fraction $f_a = n_a/2p \geq 1/2$ of such electrons is plotted in figures 5(a) and 6(a). For $t' = 3$ and $\eta = 2$ in figure 6(a), f_a has a maximum of 0.564 in zero field and approaches $1/2$ as $B' \rightarrow B'_c \approx 4.8$. Similar behaviour is found in figure 5(a), where f_a is shown to be an increasing function of η above $\eta_c \approx 1.6$. In [25], it was shown that f_a decreases with t' and approaches $1/2$ as $t' \rightarrow t'_c$.

This behaviour is easy to understand: the largest angles between neighbouring spins are along the x axis between b sites with angles differing by $2\theta_b$. When an electron hops onto a b site, it cannot easily hop to other b sites and so quickly moves on to a neighbouring a site, where it can readily travel between other a sites with angular difference $2\theta_a \ll 2\theta_b$. Hence, the non-collinearity of the local moments quite naturally produces a charge-density wave (CDW) with a substantial amplitude. As $\eta \rightarrow \infty$, θ_b approaches $\pi/2$ and f_a approaches 0.593. So even when the electrons are unable to hop between sites on the b sublattice (since the angles on neighbouring b sites differ by π), roughly 40% of the electrons can still be found on b sites at any one time. Because neither the CAF nor FM densities-of-states contain a gap, both phases are metallic within the DEV model for $t' > 0$.

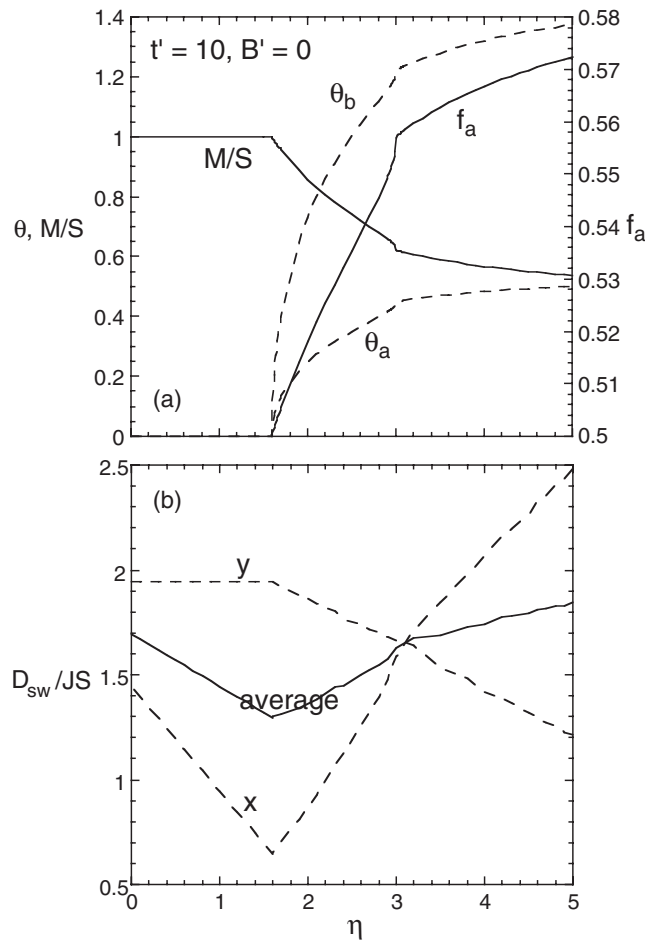


Figure 5. (a) The angles θ_a and θ_b of the local moments, the total local magnetization M/S , the fraction f_a of the electrons on the a sites, and (b) the spin-wave stiffnesses for $p = 0.66$, $t' = 10$ and $B' = 0$ versus η .

Due to short-range orbital ordering, a CDW with the same period as the one predicted here has in fact been observed in the AFM regions of $\text{Pr}_{0.7}\text{Ca}_{0.3}\text{MnO}_3$ [7, 29]. However, the observed charge ordering is perfect: all of the Mn^{3+} ions lie on one sublattice and all of the Mn^{4+} ions lie on the other. Such perfect charge ordering is never achieved within the DEV model.

Another surprising result is that phase separation occurs within a narrow range of t' . In a plot of filling p versus chemical potential μ , phase separation appears as a jump Δp in $p(\mu)$. For the parameters $\eta = 3$ and $B = 0$ in figure 7, Δp reaches a maximum of about 0.0028 when $t' \approx 10.0$ and shrinks as t' increases. If p is fixed at 0.66, then phase separation occurs within a very narrow range of t' between about 9.98 and 10.02. For fixed p , phase separation appears as jumps in the equilibrium angles θ_r and in the electron fraction f_a , as seen in figure 5(a) for zero field.

Like the Pomeranchuk instability [30, 31] in the two-dimensional Hubbard model, the phase instability in the DEV model occurs close to, but slightly above, the Van Hove filling and is marked by a change in Fermi surface (FS) topology from closed to open. In the usual Pomeranchuk instability, however, the change in FS topology spontaneously breaks the square symmetry of the lattice. Square symmetry is already broken in the DEV model by the Villain arrangement of the Heisenberg interactions. The FS of the DEV model is sketched in figure 8

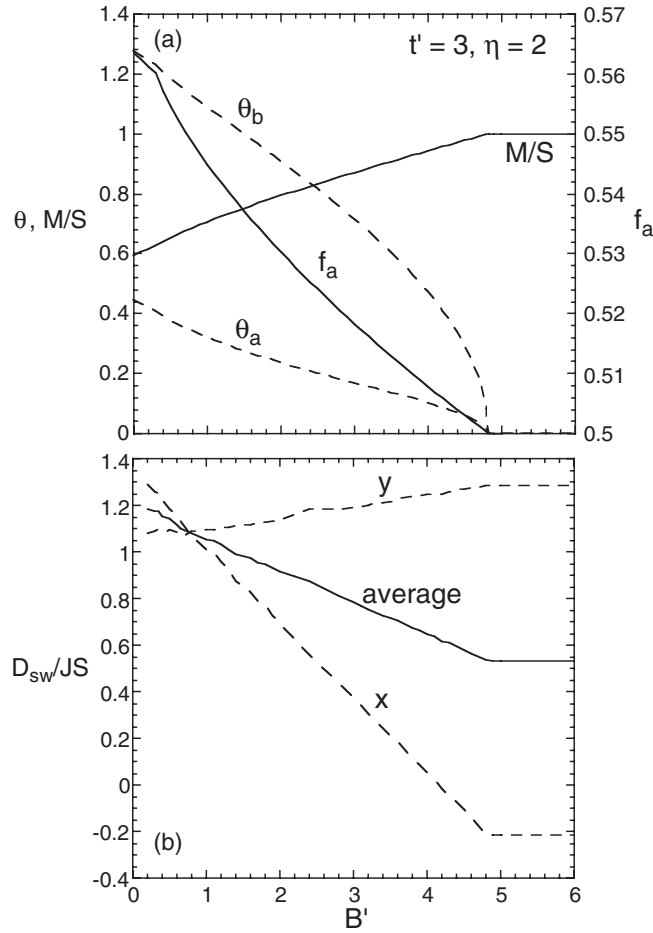


Figure 6. (a) The angles θ_a and θ_b of the local moments, the total local magnetization M/S and the fraction f_a of the electrons on the a sites, and (b) the spin-wave stiffnesses for $p = 0.66$, $t' = 3$ and $\eta = 2$ versus B' .

for $\eta = 3$, $B = 0$, $p = 0.66$, and for values of t' on either side of the phase-separated range. For t' just above 10.0, the extra electrons in the neck of the a FS around $\mathbf{k} = 0$ are offset by the holes in the b FS around $\mathbf{k} = (\pi, \pi/2)$. Although phase separation occurs for any t' around some value of the filling, it becomes significant only if the b FS is already present when the necks in the a FS develop. For the parameters in figure 7, this requires that $t' \geq 9.9$.

A magnetic field very quickly narrows and then eliminates the region of phase separation. For $t' = 3$ and $\eta = 2$, phase separation does not occur with increasing field. The small kinks in the equilibrium angles and electron fraction seen in figure 6(a) correspond to points of Van Hove filling (where the necks in the a FS first appear) but not to a phase-separated region.

4. Spin dynamics of the DEV model

In this section, we evaluate the SW frequencies for the DEV model by following the general formalism developed by Golosov [23]. While introducing some new physics, the presence of non-collinear spins also complicates things a bit.

When $J_H S/t$ is finite, the relationships given above for $\bar{c}_{\mathbf{k}\alpha}^{(r)}$ in terms of $d_{\mathbf{k}\alpha}^{(s)}$ must contain admixtures of the opposite-spin terms $(t/J_H S)d_{\mathbf{k}+\mathbf{Q},-\alpha}^{(s)}$. As sketched in figure 1(c), this implies that the equilibrium angles ψ_r of the electrons are smaller than the angles θ_r of the local

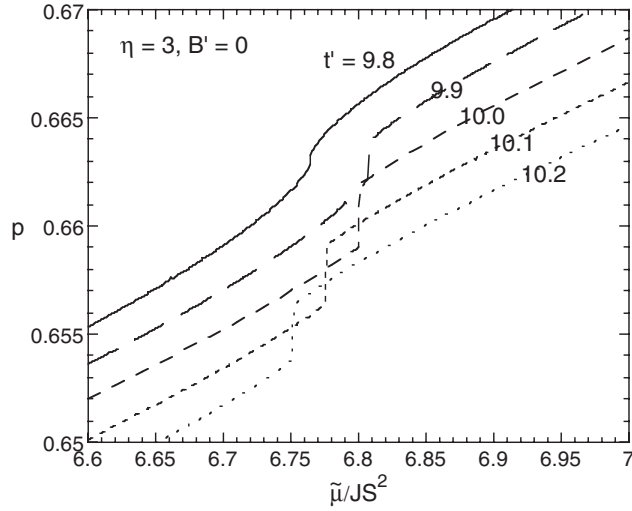


Figure 7. The filling p versus shifted chemical potential $\tilde{\mu} = \mu + J_{\text{H}}S$ for various values of t' , $\eta = 3$ and $B' = 0$. Phase separation appears as discontinuities in p .

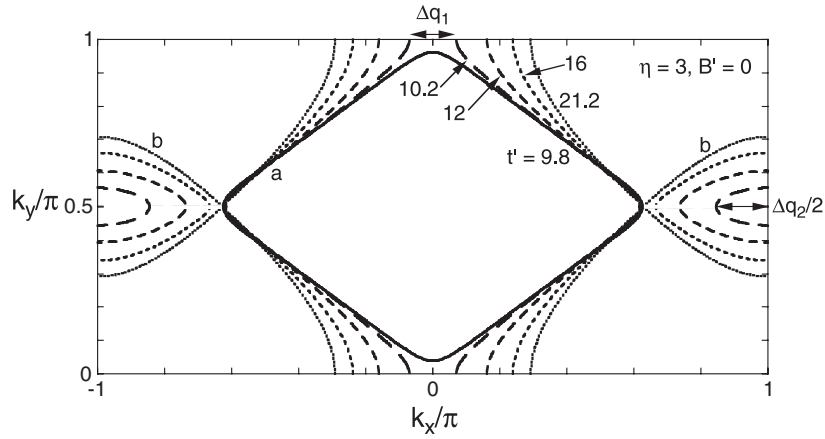


Figure 8. The FS is plotted for $\eta = 3$, $B' = 0$, $p = 0.66$, and $t' = 9.8, 10.2, 12, 16$ or 21.2 . For $t' > 10$, the a FS develops necks around $\mathbf{k} = 0$.

moments because the electrons try to align their spins as much as possible. For large Hund's coupling, $\theta_r - \psi_r \propto t/J_{\text{H}}S$ and the electrons always exert a small torque on the local moments. In the local reference frame of site i on the r sublattice, $\langle \bar{s}_{ix} \rangle = (n_r/2) \sin(\theta_r - \psi_r)$ so these new terms produce a correction to the Hund's coupling $-J_{\text{H}}\mathbf{S}_i \cdot \mathbf{s}_i$ that survives in the $J_{\text{H}}S \rightarrow \infty$ limit. Indeed, these torque terms are required to obtain sensible results for the SW frequencies.

To second order in perturbation theory, the new relationships for the Fermion operators are given by

$$\bar{c}_{\mathbf{k}\alpha}^{(a)} = u_{\mathbf{k}}^{(a)} d_{\mathbf{k}\alpha}^{(a)} + u_{\mathbf{k}}^{(b)} d_{\mathbf{k}\alpha}^{(b)} + \frac{t}{J_{\text{H}}S} \left\{ (u_{\mathbf{k}}^{(a)} \cos k_y \sin((\theta_a - \theta_b)/2) - u_{\mathbf{k}}^{(b)} \cos k_x \sin \theta_a) d_{\mathbf{k}+\mathbf{Q},-\alpha}^{(a)} - (u_{\mathbf{k}}^{(a)} \cos k_x \sin \theta_a + u_{\mathbf{k}}^{(b)} \cos k_y \sin((\theta_a - \theta_b)/2)) d_{\mathbf{k}+\mathbf{Q},-\alpha}^{(b)} \right\}, \quad (18)$$

$$\bar{c}_{\mathbf{k}\alpha}^{(b)} = u_{\mathbf{k}}^{(b)} d_{\mathbf{k}\alpha}^{(a)} - u_{\mathbf{k}}^{(a)} d_{\mathbf{k}\alpha}^{(b)} + \frac{t}{J_{\text{H}}S} \left\{ -(u_{\mathbf{k}}^{(a)} \cos k_x \sin \theta_b + u_{\mathbf{k}}^{(b)} \cos k_y \sin((\theta_a - \theta_b)/2)) d_{\mathbf{k}+\mathbf{Q},-\alpha}^{(a)} + (-u_{\mathbf{k}}^{(a)} \cos k_y \sin((\theta_a - \theta_b)/2) + u_{\mathbf{k}}^{(b)} \cos k_x \sin \theta_b) d_{\mathbf{k}+\mathbf{Q},-\alpha}^{(b)} \right\}. \quad (19)$$

On the r sublattice, these equations imply that $\theta_r - \psi_r$ is related to the band and harmonic energies by

$$\frac{n_r}{2} \sin(\theta_r - \psi_r) = \frac{1}{J_H S} \frac{d}{d\theta_r} \frac{E_b}{N} = -\frac{1}{J_H S} \frac{d}{d\theta_r} \frac{E_h}{N}, \quad (20)$$

which can also be obtained by minimizing the classical energy $\mathcal{E}(\theta_a, \theta_b) = -J_H S \sum_i n_i \cos(\theta_i - \psi_i) + E_h(\theta_a, \theta_b)$ with respect to θ_a or θ_b . Hence, the torque exerted by the electrons on the local moments opposes the tendency of the local moments to return to the angles that minimize E_h .

In terms of the Fermion operators $d_{\mathbf{k}\alpha}^{(r)}$ and $d_{\mathbf{k}\alpha}^{(r)\dagger}$ that diagonalize H_b , the full Hamiltonian can be expanded in a power series in $1/\sqrt{S}$ as $H = H_0 + H_1 + H_2 + \dots$. The first-order term may be written

$$\begin{aligned} H_1 = & -2J_H \sqrt{\frac{S}{N}} \sum_{\mathbf{k}, \mathbf{q}, r, s} d_{\mathbf{k}+\mathbf{q}, \downarrow}^{(r)\dagger} d_{\mathbf{k}, \uparrow}^{(s)} \left\{ u_{\mathbf{k}+\mathbf{q}}^{(r)} u_{\mathbf{k}}^{(s)} a_{\mathbf{q}}^{(a)} + v_{\mathbf{k}+\mathbf{q}}^{(r)} v_{\mathbf{k}}^{(s)} a_{\mathbf{q}}^{(b)} \right\} \\ & - \frac{2t}{\sqrt{SN}} \sum_{\mathbf{k}, \mathbf{q}, r, s} \left\{ d_{\mathbf{k}+\mathbf{q}, \uparrow}^{(r)\dagger} d_{\mathbf{k}+\mathbf{Q}, \uparrow}^{(s)} (u_{\mathbf{k}+\mathbf{q}}^{(r)} x_{\mathbf{k}}^{(s)} a_{\mathbf{q}}^{(a)} + v_{\mathbf{k}+\mathbf{q}}^{(r)} y_{\mathbf{k}}^{(s)} a_{\mathbf{q}}^{(b)}) \right. \\ & \left. + d_{\mathbf{k}+\mathbf{q}+\mathbf{Q}, \downarrow}^{(r)\dagger} d_{\mathbf{k}, \downarrow}^{(s)} (u_{\mathbf{k}}^{(s)} x_{\mathbf{k}+\mathbf{q}}^{(r)} a_{\mathbf{q}}^{(a)} + v_{\mathbf{k}}^{(s)} y_{\mathbf{k}+\mathbf{q}}^{(r)} a_{\mathbf{q}}^{(b)}) \right\} + \text{h.c.}, \quad (21) \end{aligned}$$

where

$$x_{\mathbf{k}}^{(a)} = u_{\mathbf{k}}^{(a)} \cos k_y \sin((\theta_a - \theta_b)/2) - u_{\mathbf{k}}^{(b)} \cos k_x \sin \theta_a, \quad (22)$$

$$y_{\mathbf{k}}^{(a)} = -u_{\mathbf{k}}^{(b)} \cos k_y \sin((\theta_a - \theta_b)/2) - u_{\mathbf{k}}^{(a)} \cos k_x \sin \theta_b, \quad (23)$$

and $x_{\mathbf{k}}^{(b)} = -x_{\mathbf{k}+\mathbf{Q}}^{(a)}$, $y_{\mathbf{k}}^{(b)} = y_{\mathbf{k}+\mathbf{Q}}^{(a)}$, $v_{\mathbf{k}}^{(a)} = u_{\mathbf{k}}^{(b)}$, and $v_{\mathbf{k}}^{(b)} = -u_{\mathbf{k}}^{(a)}$. The second term in equation (21) is produced by the torque exerted by the electrons on the local moments. Notice that H_1 is linear in the boson operators. The expectation value of the Fermion factor multiplying the boson operators in equation (21) vanishes provided that θ_r satisfy equations (13) and (14). The second-order Hamiltonian can be written as

$$H_2 = \frac{2J_H}{N} \sum_{\mathbf{k}, \mathbf{q}_1, \mathbf{q}_2, r, s} \sum_{\alpha, \beta} \sigma_{\alpha\beta}^z d_{\mathbf{k}-\mathbf{q}_1, \alpha}^{(r)\dagger} d_{\mathbf{k}-\mathbf{q}_2, \beta}^{(s)} \left\{ a_{\mathbf{q}_1}^{(a)\dagger} a_{\mathbf{q}_2}^{(a)} u_{\mathbf{k}-\mathbf{q}_1}^{(r)} u_{\mathbf{k}-\mathbf{q}_2}^{(s)} + a_{\mathbf{q}_1}^{(b)\dagger} a_{\mathbf{q}_2}^{(b)} v_{\mathbf{k}-\mathbf{q}_1}^{(r)} v_{\mathbf{k}-\mathbf{q}_2}^{(s)} \right\}. \quad (24)$$

Since J_H/J_S and t/J_S are of the order of S^0 , H_1/J_S^2 is of the order of $1/\sqrt{S}$ and H_2/J_S^2 is of the order of $1/S$.

To eliminate the first-order term in H and to express the Hamiltonian in terms of the true SW operators for the total spin $\mathbf{S}_{i, \text{tot}} = \mathbf{S}_i + \mathbf{s}_i$, we perform the unitary transformation [23] $H' = e^{-U} H e^U$ where U is constructed to satisfy $[U, H_0] = H_1$. This transformation produces a modified second-order term $H'_2 = H_2 + [U, H_1]/2$. The anti-Hermitian operator U that fulfills these requirements is

$$\begin{aligned} U = & -2J_H \sqrt{\frac{S}{N}} \sum_{\mathbf{k}, \mathbf{q}, r, s} d_{\mathbf{k}+\mathbf{q}, \downarrow}^{(r)\dagger} d_{\mathbf{k}, \uparrow}^{(s)} (a_{\mathbf{q}}^{(a)} u_{\mathbf{k}+\mathbf{q}}^{(r)} u_{\mathbf{k}}^{(s)} + a_{\mathbf{q}}^{(b)} v_{\mathbf{k}+\mathbf{q}}^{(r)} v_{\mathbf{k}}^{(s)}) \frac{1}{\tilde{\epsilon}_{\mathbf{k}}^{(s)} - \tilde{\epsilon}_{\mathbf{k}+\mathbf{q}}^{(r)} - 2J_H S} \\ & - \frac{2t}{\sqrt{SN}} \sum_{\mathbf{k}, \mathbf{q}, r, s} \left\{ d_{\mathbf{k}+\mathbf{q}, \uparrow}^{(r)\dagger} d_{\mathbf{k}+\mathbf{Q}, \uparrow}^{(s)} (a_{\mathbf{q}}^{(a)} u_{\mathbf{k}+\mathbf{q}}^{(r)} x_{\mathbf{k}}^{(s)} + a_{\mathbf{q}}^{(b)} v_{\mathbf{k}+\mathbf{q}}^{(r)} y_{\mathbf{k}}^{(s)}) \right. \\ & \left. + d_{\mathbf{k}+\mathbf{q}, \downarrow}^{(r)\dagger} d_{\mathbf{k}+\mathbf{Q}, \downarrow}^{(s)} (a_{\mathbf{q}}^{(a)} u_{\mathbf{k}+\mathbf{Q}}^{(s)} x_{\mathbf{k}+\mathbf{q}+\mathbf{Q}}^{(r)} + a_{\mathbf{q}}^{(b)} v_{\mathbf{k}+\mathbf{Q}}^{(s)} y_{\mathbf{k}+\mathbf{q}+\mathbf{Q}}^{(r)}) \right\} \frac{1}{\tilde{\epsilon}_{\mathbf{k}+\mathbf{Q}}^{(s)} - \tilde{\epsilon}_{\mathbf{k}+\mathbf{q}}^{(r)}} - \text{h.c.}, \quad (25) \end{aligned}$$

which is clearly of the order of $(J_S^2)/\sqrt{S}$.

Performing the unitary transformation and taking the limit $J_{\text{H}}S \rightarrow \infty$ produces a rather complicated expression for H'_2 . This expression can be considerably simplified by tracing over the Fermion degrees of freedom, thereby replacing the combination of Fermi operators $d_{\mathbf{k}\uparrow}^{(r)\dagger} d_{\mathbf{k}'\uparrow}^{(s)}$ by its expectation value $\delta_{r,s} \delta_{\mathbf{k},\mathbf{k}'} f(\tilde{\epsilon}_{\mathbf{k}}^{(r)})$. Then H'_2 can be written as an effective Hamiltonian for the SW operators $a_{\mathbf{k}}^{(r)}$ and $a_{\mathbf{k}}^{(r)\dagger}$ that takes the same form as the harmonic Hamiltonian of equation (6) but with revised coefficients given in appendix A. The SW frequency $\omega_{\mathbf{k}}$ is given by equation (A.10) with $\tilde{A}_{\mathbf{k}}^{(r,s)}$ and $\tilde{B}_{\mathbf{k}}^{(r,s)}$ replacing the harmonic coefficients.

Note that the torque terms in H_1 produce the corrections $D_{\mathbf{k}}^{(r,s)}$ and $E_{\mathbf{k}}^{(r,s)}$ (given by equations (A.7) and (A.8)) to the harmonic coefficients. Both sets of terms vanish in the FM phase, leaving only the correction $C_{\mathbf{k}}^{(r,s)}$ to $\tilde{A}_{\mathbf{k}}^{(r,s)}$. But in the CAF phase, these corrections are required to preserve rotational symmetry and the relations $\omega_{\mathbf{Q}} = 0$ and $\omega_0 = B$.

An analytic expression for the SW frequency is possible in the FM phase:

$$\omega_{\mathbf{k}} = B + JS(3 - \eta + (\eta - 1) \cos k_x) + K(2 - \cos k_x)/4S - JS \sqrt{(1 + \eta)^2 (1 - \cos k_x)^2 + (2 + K/4JS^2)^2 \cos^2 k_y}, \quad (26)$$

which generalizes equation (7) for the Villain model. The FM phase becomes unstable when $\omega_{\mathbf{Q}} = 0$, which yields the same condition for the CAF–FM phase boundary as equation (15). In the FM phase, the SW stiffnesses are the sum of DE and Heisenberg contributions: $D_{\text{sw}}^x = K/8S + JS(1 - \eta)/2$ and $D_{\text{sw}}^y = K/8S + JS$, both independent of field. For $J = 0$, these results agree with the SW frequencies of the DE model first obtained by Furukawa [32]. When $\eta = -1$, the SWs are isotropic because all nearest-neighbour interactions equal J .

In the CAF phase, the SW frequency and stiffnesses are solved numerically by integrating over the first Brillouin zone to obtain $C_{\mathbf{k}}^{(r,s)}$, $D_{\mathbf{k}}^{(r,s)}$ and $E_{\mathbf{k}}^{(r,s)}$. The changes in the SW frequency with increasing t' were discussed in [25] for $\eta = 3$ and $B = 0$. For all $t' \leq t'_c \approx 21.2$, the SW frequency vanishes at both the FM and AFM Bragg vectors. Above the phase separation region around $t' \approx 10.0$ but below t'_c , $\omega_{\mathbf{k}}$ develops kinks that correspond to transitions across the neck of the a FS ($\Delta \mathbf{q}_1 = \mathbf{Q} - \mathbf{k}_1$) and across the length of the b FS ($\Delta \mathbf{q}_2 = \mathbf{Q} - \mathbf{k}_2$). These transitions are sketched in figure 8. Since the nesting across $\Delta \mathbf{q}_2$ is much weaker than across $\Delta \mathbf{q}_1$, the kink in the SW frequency at \mathbf{k}_2 is much weaker than the one at \mathbf{k}_1 . As $t' \rightarrow 10.0$, $\Delta \mathbf{q}_i \rightarrow 0$ so the kinks at \mathbf{k}_1 and \mathbf{k}_2 merge with \mathbf{Q} . Whereas $\omega_{\mathbf{k}}$ is a non-monotonic function of t' along the x direction, it is a monotonically increasing function of t' along the y direction.

As plotted in figure 2 of [25] for $\eta = 3$ and $B' = 0$, the SW stiffness in the x direction reaches a minimum at t'_c , above which both D_{sw}^x and D_{sw}^y are linearly increasing functions of t' . The stiffnesses in the x and y directions cross in the region of phase separation, where the SWs become isotropic. For $\eta = 3$ and $B' = 0$, the average SW stiffness $D_{\text{sw}}^{\text{av}}$ doubles as t' increases from zero to t'_c .

With increasing η , the SW stiffnesses plotted in figure 5(b) for $t' = 10$ and $B = 0$ again cross in the region of phase separation around $\eta = 3.0$. For larger η , $D_{\text{sw}}^x > D_{\text{sw}}^y$. Due to the strong increase in D_{sw}^x with η , the average SW stiffness actually grows as the local moments become more non-collinear. Similar behaviour was found when $t = 0$ in figure 2, where $D_{\text{sw}}^{\text{av}}$ was also found to be an increasing function of η . The SW frequencies are plotted for $t' = 10$, $B' = 0$ and various values of η in figure 9(a). As shown, the SW frequency softens at \mathbf{Q} as η approaches the critical value of 1.6. The kinks in the SW spectrum at \mathbf{k}_1 and \mathbf{k}_2 are clearly seen for $\eta = 2.9$. Otherwise, the behaviour of the SW frequencies is very similar to that shown in figure 4(a) in the absence of electron hopping.

The effect of a magnetic field is demonstrated in figures 6(b) and 9(b) for $\eta = 2$ and $t' = 3$. Absent from figure 6(b) is the region of very low fields, where the behaviour of the SW stiffness is complicated by the dependence of the function $D_{\text{sw}}^{\alpha}(k_{\alpha}, B) = (\omega_{\mathbf{k}} - B)/k_{\alpha}^2$ on

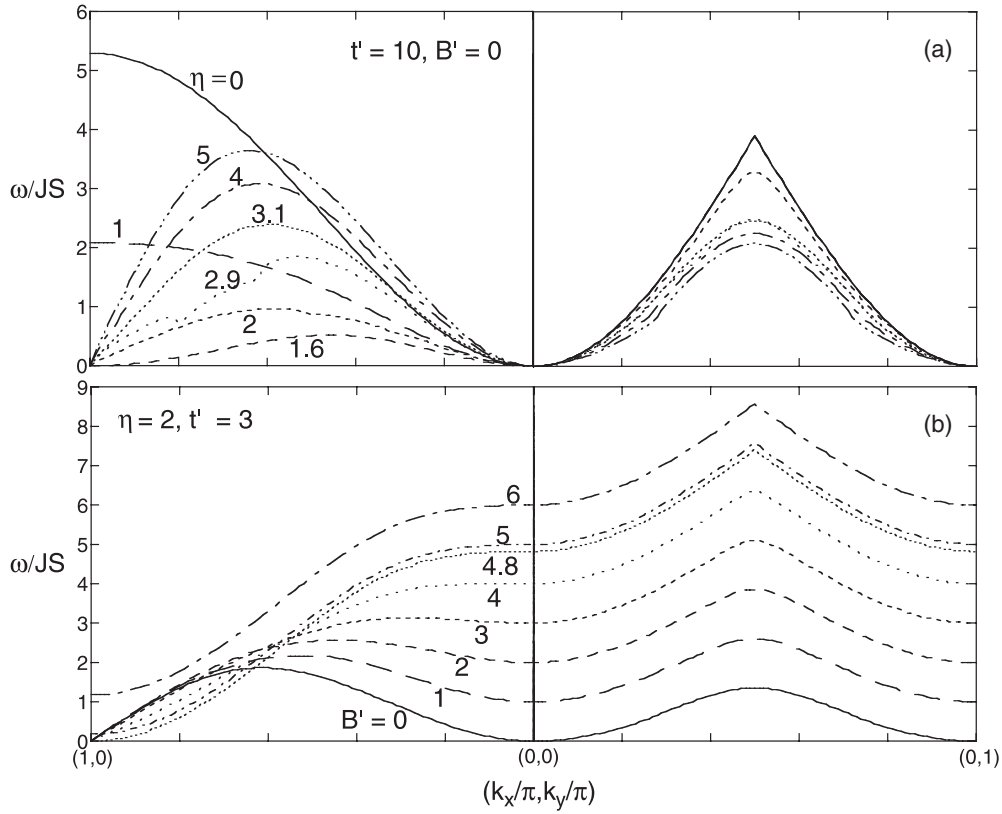


Figure 9. (a) The SW frequencies for $p = 0.66$, $t' = 3$, $B' = 0$ and various values of η , and (b) the SW frequencies for $p = 0.66$, $\eta = 2$, $t' = 3$ and various values of B' .

the ratio $k_\alpha/\sqrt{B'}$ [27]. For larger fields, there is a gradual increase in D_{sw}^y and a decrease in D_{sw}^x as B grows from 0 to $B_c \approx 4.8JS$. The drop in D_{sw}^x with field is caused by the growth of the SW gap $\omega_0 = B$ at $\mathbf{k} = 0$, while the SW frequency continues to vanish at $\mathbf{Q} = (\pi, 0)$ for $B < B_c$, as seen in figure 9(b). Hence, the average SW stiffness drops from roughly $1.2JS$ at $B = 0$ to $0.54JS$ at B_c . Because a magnetic field very quickly destroys the region of phase separation, the crossing point of the x and y stiffnesses does not coincide with a region of phase separation. As expected, the SW stiffnesses are independent of field above B_c . Notice from figures 9(a) and (b) that the SW velocity at \mathbf{Q} softens within the CAF phase as t approaches t_c or B approaches B_c . This behaviour occurs at the CAF–FM phase boundary of any magnetic system [28].

5. Discussion and conclusion

Applying the results of this work to the manganites requires an estimation of the relevant parameters. Using $S = 3/2$, $\eta JS \approx 8.6$ meV, $\eta \sim 1$ [33] and $t \approx 200$ meV for the metallic phase gives $t' \approx 32$ and $B' \approx 0.028B(T)$. When $\eta = 1$, the critical values of the DEV model are $t'_c = 5.3$ in zero field and $B'_c = 2.5$ for $t' = 0$. Hence, the metallic value for the hopping energy is more than sufficient to stabilize the FM phase but an applied field of 3 T cannot align the local moments when t' is much below t'_c .

Metal–insulator transitions in many of the manganites have been successfully interpreted within the framework of percolation theory [34, 35]. When the FM fraction f exceeds a critical value f_c , a FM backbone spans the sample and the system becomes metallic. The percolation threshold f_c in those manganites lies between 0.17 and 0.19. But it is rather difficult to explain the jump in the SW stiffness observed in $\text{Pr}_{0.7}\text{Ca}_{0.3}\text{MnO}_3$ [11] within the framework of percolation theory. Assuming that the metal–insulator transition in $\text{Pr}_{1-x}\text{Ca}_x\text{MnO}_3$ is produced by the percolation of metallic FM clusters [10], there is no reason why the SW stiffness should change when a FM backbone spans the sample. Within percolation theory, one would more naturally expect the SW stiffness to gradually increase with field as a growing fraction of the sample becomes metallic.

Estimates of the FM fraction f in $\text{Pr}_{1-x}\text{Ca}_x\text{MnO}_3$ manganites also pose a difficulty for percolation theory. The accepted range for the percolation threshold f_c within continuum models falls between 0.15 and 0.22. While one experimental estimate of $f_c \approx 0.08$ [10] at the metal–insulator transition lies well below this accepted range, a recent estimate of $f_c \approx 0.6$ [13] based on more complete magnetization data lies well above this range. At zero field and low temperatures, estimates for f range from 0.3 [13] to 0.5 [9]. If those estimates are correct and the FM regions are metallic, then the percolation threshold would already be exceeded and the low-temperature phase would be metallic in zero field.

On the other hand, our results clearly indicate that the jump in the SW stiffness at a field of 3 T cannot be produced by simply aligning the AFM regions while keeping the bandwidth $\sim t$ fixed. As found in figure 6(b), a magnetic field would act to suppress rather than enhance the average SW stiffness under those conditions. Moreover, a field of 3 T corresponding to $B' \approx 0.086 \ll B'_c$ will have little effect on the alignment of the local moments. Whereas experiments indicate that the AFM regions begin to shrink under a magnetic field greater than 3 T, a sizeable fraction of the sample remains AFM even above the metal–insulator transition [10, 11, 13].

The large increase in the SW stiffness predicted by our work as t' increases from 0 to t'_c suggests an entirely different scenario: at the critical field, electrons in the insulating and possibly canted FM regions delocalize as the hopping energy t sharply increases. Since the integrated optical weight is just $K \sim t$, the jump in the hopping energy at 3 T should be observable in optical measurements. Indeed, measurements by Okimoto *et al* [7] on $\text{Pr}_{0.6}\text{Ca}_{0.4}\text{MnO}_3$ reveal a rapid rise in $\sigma(\omega)$ and a rapid drop in the CDW gap near the critical field. If the percolation threshold for the FM regions is exceeded when the electrons delocalize, as suggested by the measurements discussed above, then the jump in the SW stiffness will coincide with the metal–insulator transition. Otherwise, the metal–insulator transition will occur at a slightly larger field.

Supporting this picture are the plethora of probes that can produce a metal–insulator transition in $\text{Pr}_{1-x}\text{Ca}_x\text{MnO}_3$ ($0.3 \leq x \leq 0.4$). Besides a magnetic field, application of an electric field [36], high pressure [37], exposure to x-rays [38] and exposure to visible light [39] all induce a metal–insulator transition. The identical resistivities produced by application of a magnetic field or exposure to x-rays [38] suggest a common mechanism: the excitation of charge carriers out of polaronic traps produced by the electron–lattice coupling. The subsequent relaxation of the lattice [9, 38] may prevent retrapping of the electrons.

The jump in the SW stiffness as a function of field in $\text{Pr}_{0.7}\text{Ca}_{0.3}\text{MnO}_3$ [11] also bears a striking resemblance to the jump in the SW stiffness observed in $\text{La}_{1-x}\text{Ca}_x\text{MnO}_3$ at the metal–insulator transition with $x \approx 0.22$ [40]. In fact, the sizes of the SW stiffnesses on either side of the doping-induced transition in $\text{La}_{1-x}\text{Ca}_x\text{MnO}_3$ are almost exactly the same as on either side of the field-induced transition in $\text{Pr}_{0.7}\text{Ca}_{0.3}\text{MnO}_3$. This suggests that there are also

large increases in the hopping energy and electronic kinetic energy in $\text{La}_{1-x}\text{Ca}_x\text{MnO}_3$ at the critical concentration of $x \approx 0.22$.

Compare the jump in the SW stiffness across the metal–insulator transition with the smooth dependence of the spin-diffusion coefficient Λ [4, 40], which gives the lifetime $\tau(\mathbf{k}) = 1/\Lambda k^2$ of paramagnetic spin fluctuations. Measurements [40] of the spin-diffusion coefficient were performed just below T_C , where paramagnetic spin relaxation occurs within polaronic regions of the FM phase. While D_{sw} is a linear function of the electronic kinetic energy in the FM phase, $\Lambda \chi$ depends only on doping and is independent of the electronic bandwidth W in the low-temperature limit $T \ll W$ [4]. So long as the bandwidth of the polaronic regions remains large compared to the temperature, the spin-diffusion coefficient will not change across the metal–insulator transition.

Except in a very narrow range of parameters, phase separation is absent in the DEV model. Phase separation appears quite commonly in DE models with AFM Heisenberg interactions [1] and even occurs near $p = 1$ in a DE model without Heisenberg interactions [41]. Results for the DEV model contrast with both a DE model with AFM interactions between all neighbouring local moments [20–23] and a DE model with FM interactions in plane but AFM interactions between neighbouring planes [42]. Due to the high symmetry of both models, AFM order is not frustrated when $t = 0$. But in both cases, phase separation occurs before the AFM interactions become strong enough to cant the spins. Work by Golosov [21, 23] indicates that the canted phase is destabilized by the presence of local degeneracies (see footnote 1) that are absent in the DEV model. Our results suggest that phase separation only occurs within a very narrow range of parameters when the AFM Heisenberg interactions are frustrated and local degeneracies are absent. For doping concentrations away from multiples of a quarter filling, long-range orbital ordering is impossible and magnetic frustration may be present in a wide range of manganites. Therefore, the DE model may not provide as straightforward a pathway to phase separation in the manganites as believed. A much more important role may be played by the quenched disorder associated with chemical inhomogeneities [43].

Román and Soto [28] pointed out that the nature of the FM and AFM regions can be probed by measuring the SW spectrum about the AFM Bragg vector \mathbf{Q} . In a CAF, the SWs at \mathbf{Q} are not gapped for any field B below B_c , as shown in figures 4(b) and 9(b). But in a phase-separated mixture, the SW branch of the FM regions will not vanish at \mathbf{Q} . As discussed elsewhere [27] and seen in the inset to figure 3(b), the rapid increase in the SW stiffness for fields near B^* is another signature of a canted phase.

Since CE-type AFM ordering occurs at half-filling, the local charge ordering observed in the manganites $\text{Pr}_{0.6}\text{Ca}_{0.4}\text{MnO}_3$ [7, 29] and $\text{La}_{0.7}\text{Ca}_{0.3}\text{MnO}_3$ [2, 3] would be simplified if the polaronic regions were rich in holes and poor in electrons compared to the bulk. Our model provides a natural explanation for this behaviour, since the electronic fraction on b sites is substantially smaller than the fraction on a sites as the electrons avoid regions with more pronounced AFM order.

This paper has studied the general effects of AFM interactions and non-collinearity on the magnetic ordering and spin dynamics of DE systems. The competition between DE and AFM interactions is responsible for several interesting properties. In a narrow region of hopping energies, weak phase separation occurs as the FS topology changes from closed to open. Because electrons prefer to occupy sites that are coupled by FM interactions, a CDW appears in the absence of a CDW gap. For finite Hund's coupling, the electron spins are more closely aligned than the local moments of the CAF. The CAF becomes unstable above critical values of field and hopping energy and below a critical value of η . Perhaps the most surprising result is that DE changes none of the qualitative features of the CAF state. The SW gap ω_0 at $\mathbf{k} = 0$ remains equal to B and the gap $\omega_{\mathbf{Q}}$ at the AFM Bragg vector \mathbf{Q} continues to vanish

for any hopping energy below t_c . The average SW stiffness still softens with magnetic field and hardens with strengthening AFM interactions; the SW velocity at \mathbf{Q} still vanishes at the CAF–FM transition. Clearly, a great deal can be learned about the general properties of CAFs, even of the more complex variations that appear in many manganites, by considering simple models such as the DEV model.

Acknowledgments

It is a pleasure to acknowledge helpful conversations with Drs A Chernyshev, P-C Dai, E Dagotto, J Fernandez-Baca, D Golosov, M Katsnelson, N Furukawa, W Saslow and A Zheludev. This research was sponsored by the US Department of Energy under contract DE-AC05-00OR22725 with Oak Ridge National Laboratory, managed by UT-Battelle, LLC.

Appendix A

The coefficients of the harmonic Hamiltonian of the generalized Villain model (equation (6)) are

$$A_{\mathbf{k}}^{(a,a)} = 2 \cos 2\theta_a + 2 \cos(\theta_a - \theta_b) - 2 \cos^2 \theta_a \cos k_x + B' \cos \theta_a, \quad (\text{A.1})$$

$$A_{\mathbf{k}}^{(a,b)} = A_{\mathbf{q}}^{(b,a)} = -2 \cos^2((\theta_a - \theta_b)/2) \cos k_y, \quad (\text{A.2})$$

$$A_{\mathbf{k}}^{(b,b)} = 2 \cos(\theta_a - \theta_b) - 2\eta \cos 2\theta_b + 2\eta \cos^2 \theta_b \cos k_x + B' \cos \theta_b, \quad (\text{A.3})$$

$$B_{\mathbf{k}}^{(a,a)} = \sin^2 \theta_a \cos k_x, \quad (\text{A.4})$$

$$B_{\mathbf{k}}^{(a,b)} = B_{\mathbf{k}}^{(b,a)} = \sin^2((\theta_a - \theta_b)/2) \cos k_y, \quad (\text{A.5})$$

$$B_{\mathbf{k}}^{(b,b)} = -\eta \sin^2 \theta_b \cos k_x, \quad (\text{A.6})$$

where the lattice constant is set to one.

For the DEV model, the revised coefficients of the harmonic Hamiltonian are $\tilde{A}_{\mathbf{k}}^{(r,s)} = A_{\mathbf{k}}^{(r,s)} + C_{\mathbf{k}}^{(r,s)} + D_{\mathbf{k}}^{(r,s)}$ and $\tilde{B}_{\mathbf{k}}^{(r,s)} = B_{\mathbf{k}}^{(r,s)} + E_{\mathbf{k}}^{(r,s)}$, with new contributions

$$C_{\mathbf{k}}^{(r,s)} = -\frac{1}{N} \sum_{\mathbf{q},l} f(\tilde{\epsilon}_{\mathbf{q}}^{(l)}) \left\{ u_{\mathbf{q}}^{(l)2} (2t' \cos \theta_a \cos(k_x + q_x) + \tilde{\epsilon}_{\mathbf{q}}^{(l)}) \delta_{r,a} \delta_{s,a} \right. \\ \left. + v_{\mathbf{q}}^{(l)2} (2t' \cos \theta_b \cos(k_x + q_x) + \tilde{\epsilon}_{\mathbf{q}}^{(l)}) \delta_{r,b} \delta_{s,b} \right. \\ \left. + 2t' \cos((\theta_a - \theta_b)/2) \cos(k_y + q_y) u_{\mathbf{q}}^{(l)} v_{\mathbf{q}}^{(l)} (\delta_{r,a} \delta_{s,b} + \delta_{r,b} \delta_{s,a}) \right\}, \quad (\text{A.7})$$

$$D_{\mathbf{k}}^{(r,s)} = \frac{4t'^2 J S^2}{N} \sum_{\mathbf{q},l,m} (u_{\mathbf{k}+\mathbf{q}}^{(l)} x_{\mathbf{q}}^{(m)} \delta_{r,a} + v_{\mathbf{k}+\mathbf{q}}^{(l)} y_{\mathbf{q}}^{(m)} \delta_{r,b}) \\ \times (u_{\mathbf{k}+\mathbf{q}}^{(l)} x_{\mathbf{q}}^{(m)} \delta_{s,a} + v_{\mathbf{k}+\mathbf{q}}^{(l)} y_{\mathbf{q}}^{(m)} \delta_{s,b}) \frac{f(\tilde{\epsilon}_{\mathbf{q}+\mathbf{Q}}^{(m)}) - f(\tilde{\epsilon}_{\mathbf{k}+\mathbf{q}}^{(l)})}{\tilde{\epsilon}_{\mathbf{q}+\mathbf{Q}}^{(m)} - \tilde{\epsilon}_{\mathbf{k}+\mathbf{q}}^{(l)}}, \quad (\text{A.8})$$

$$E_{\mathbf{k}}^{(r,s)} = \frac{2t'^2 J S^2}{N} \sum_{\mathbf{q},l,m} (u_{\mathbf{q}+\mathbf{Q}}^{(m)} x_{\mathbf{k}+\mathbf{q}+\mathbf{Q}}^{(l)} \delta_{r,a} + v_{\mathbf{q}+\mathbf{Q}}^{(m)} y_{\mathbf{k}+\mathbf{q}+\mathbf{Q}}^{(l)} \delta_{r,b}) \\ \times (u_{\mathbf{k}+\mathbf{q}}^{(l)} x_{\mathbf{q}}^{(m)} \delta_{s,a} + v_{\mathbf{k}+\mathbf{q}}^{(l)} y_{\mathbf{q}}^{(m)} \delta_{s,b}) \frac{f(\tilde{\epsilon}_{\mathbf{q}+\mathbf{Q}}^{(m)}) - f(\tilde{\epsilon}_{\mathbf{k}+\mathbf{q}}^{(l)})}{\tilde{\epsilon}_{\mathbf{q}+\mathbf{Q}}^{(m)} - \tilde{\epsilon}_{\mathbf{k}+\mathbf{q}}^{(l)}}. \quad (\text{A.9})$$

The spin excitation frequencies are given in terms of the coefficients $A_{\mathbf{k}}^{(r,s)}$ and $B_{\mathbf{k}}^{(r,s)}$ (or in terms of the revised coefficients $\tilde{A}_{\mathbf{k}}^{(r,s)}$ and $\tilde{B}_{\mathbf{k}}^{(r,s)}$) by

$$\omega_{\mathbf{k}} = \frac{JS}{\sqrt{2}} \sqrt{A_{\mathbf{k}}^{(a,a)2} + A_{\mathbf{k}}^{(b,b)2} + 2(A_{\mathbf{k}}^{(a,b)2} - B_{\mathbf{k}}^{(a,b)2}) - 4(B_{\mathbf{k}}^{(a,a)2} + B_{\mathbf{k}}^{(b,b)2}) - R_{\mathbf{k}}}, \quad (\text{A.10})$$

$$\begin{aligned} R_{\mathbf{k}}^2 = & 4 \left\{ A_{\mathbf{k}}^{(a,a)2} + A_{\mathbf{k}}^{(b,b)2} - 4(B_{\mathbf{k}}^{(a,a)2} + B_{\mathbf{k}}^{(b,b)2}) \right\} (A_{\mathbf{k}}^{(a,b)2} - B_{\mathbf{k}}^{(a,b)2}) \\ & + \left\{ A_{\mathbf{k}}^{(a,a)2} - A_{\mathbf{k}}^{(b,b)2} - 4(B_{\mathbf{k}}^{(a,a)2} - B_{\mathbf{k}}^{(b,b)2}) \right\}^2 + 8(A_{\mathbf{k}}^{(a,a)} A_{\mathbf{k}}^{(b,b)} + 4B_{\mathbf{k}}^{(a,a)} B_{\mathbf{k}}^{(b,b)}) \\ & \times (A_{\mathbf{k}}^{(a,b)2} + B_{\mathbf{k}}^{(a,b)2}) - 32A_{\mathbf{k}}^{(a,b)} B_{\mathbf{k}}^{(a,b)} (A_{\mathbf{k}}^{(a,a)} B_{\mathbf{k}}^{(b,b)} + A_{\mathbf{k}}^{(b,b)} B_{\mathbf{k}}^{(a,a)}). \end{aligned} \quad (\text{A.11})$$

The SW frequency satisfies the condition $\omega_{\mathbf{k}=0} = B$.

Appendix B

The hopping energy of the DEV band Hamiltonian (equation (9)) has matrix elements

$$K_{\alpha\beta}^{11}(\mathbf{k}) = -K_{\alpha\beta}^{22}(\mathbf{k}) = -2t \cos k_x \cos \theta_a \delta_{\alpha\beta}, \quad (\text{B.1})$$

$$K_{\alpha\beta}^{33}(\mathbf{k}) = -K_{\alpha\beta}^{44}(\mathbf{k}) = -2t \cos k_x \cos \theta_b \delta_{\alpha\beta}, \quad (\text{B.2})$$

$$K_{\alpha\beta}^{12}(\mathbf{k}) = -K_{\alpha\beta}^{21}(\mathbf{k}) = -2ti \cos k_x \sin \theta_a \sigma_{\alpha\beta}^y, \quad (\text{B.3})$$

$$K_{\alpha\beta}^{34}(\mathbf{k}) = -K_{\alpha\beta}^{43}(\mathbf{k}) = -2ti \cos k_x \sin \theta_b \sigma_{\alpha\beta}^y. \quad (\text{B.4})$$

$$K_{\alpha\beta}^{13}(\mathbf{k}) = K_{\alpha\beta}^{24}(\mathbf{k}) = K_{\alpha\beta}^{31}(\mathbf{k}) = K_{\alpha\beta}^{42}(\mathbf{k}) = -2t \cos k_y \cos((\theta_a - \theta_b)/2) \delta_{\alpha\beta}, \quad (\text{B.5})$$

$$K_{\alpha\beta}^{14}(\mathbf{k}) = K_{\alpha\beta}^{23}(\mathbf{k}) = -K_{\alpha\beta}^{41}(\mathbf{k}) = -K_{\alpha\beta}^{32}(\mathbf{k}) = 2ti \cos k_y \sin((\theta_a - \theta_b)/2) \sigma_{\alpha\beta}^y. \quad (\text{B.6})$$

Notice that the $\sigma_{\alpha\beta}^y$ terms couple the up and down spin states.

References

- [1] For an overview of phase separation in the manganites, see Moreo A, Yunoki S and Dagotto E 1999 *Science* **283** 2034
Dagotto E, Hotta T and Moreo A 2001 *Phys. Rep.* **233** 1
- [2] Adams C P, Lynn J W, Mukovskii Y M, Arsenov A A and Shulyatev D 2000 *Phys. Rev. Lett.* **85** 3954
- [3] Koo T Y, Kiryukhin B, Sharma P A, Hill J P and Cheong S-W 2001 *Phys. Rev. B* **64** 220405
- [4] Chernyshev A and Fishman R S 2003 *Phys. Rev. Lett.* **90** 177202
- [5] Jirak Z, Krupicka S, Simsa Z, Dlouha M and Vratislav S 1985 *J. Magn. Magn. Mater.* **53** 153
- [6] Yoshizawa H, Kawano H, Tomioka Y and Tokura Y 1996 *Phys. Rev. B* **52** R13145
Yoshizawa H, Kawano H, Tomioka Y and Tokura Y 1996 *J. Phys. Soc. Japan* **65** 1043
- [7] Okimoto Y, Tomioka Y, Onose Y, Otsuka Y and Tokura Y 1999 *Phys. Rev. B* **59** 7401
- [8] Deac I G, Mitchell J F and Schiffer P 2001 *Phys. Rev. B* **63** 172408
- [9] Radaelli P G, Ibberson R M, Argyriou D N, Casalta H, Anderson K H, Cheong S-W and Mitchell J F 2001 *Phys. Rev. B* **63** 172419
- [10] Hardy V, Wahl A and Martin C 2001 *Phys. Rev. B* **64** 064402
- [11] Fernandez-Baca J A, Dai P-C, Kawano-Furukawa H, Yoshizawa H, Plummer E W, Katano S, Tomioka Y and Tokura Y 2002 *Phys. Rev. B* **66** 054434
- [12] Simon Ch, Mercone S, Guiblin N, Martin C, Brület A and André G 2002 *Phys. Rev. Lett.* **89** 207202
- [13] Mercone S, Hardy V, Martin C, Simon C, Saurel D and Brület A 2003 *Phys. Rev. B* **68** 094422
- [14] Anderson P W and Hasegawa H 1995 *Phys. Rev.* **100** 675
- [15] DeGennes P-G 1960 *Phys. Rev.* **118** 141
- [16] Villain J 1977 *J. Phys. C: Solid State Phys.* **10** 1717
- [17] Berge B, Diep H T, Ghazali A and Lallemand P 1986 *Phys. Rev. B* **34** 3177
- [18] Gabay M, Garel T, Parker G N and Saslow W M 1989 *Phys. Rev. B* **40** 264
- [19] Saslow W M and Erwin R 1992 *Phys. Rev. B* **45** 4759
- [20] Yunoki S and Moreo A 1998 *Phys. Rev. B* **58** 6403

- [21] Golosov D I, Norman M R and Levin K 1998 *Phys. Rev. B* **58** 8617
- [22] Kagan M Yu, Khomskii D I and Mostovoy M V 1999 *Eur. Phys. J. B* **12** 217
- [23] Golosov D I 2000 *Phys. Rev. Lett.* **84** 3974
Golosov D I 2000 *J. Appl. Phys.* **87** 5804
Golosov D I 2002 *J. Appl. Phys.* **91** 7508
- [24] Mizokawa T, Khomskii D I and Sawatzky G A 2000 *Phys. Rev. B* **63** 024403
- [25] Fishman R S 2004 *Phys. Rev. B* at press
- [26] Walker L R and Walstedt R E 1980 *Phys. Rev. B* **22** 3816
- [27] Fishman R S, unpublished
- [28] Román J M and Soto J 2000 *Phys. Rev. B* **62** 3300
- [29] Asaka T, Yamada S, Tsutsumi S, Tsurata C, Kimoto K, Arima T and Matsui Y 2002 *Phys. Rev. Lett.* **88** 097201
- [30] Halboth C J and Metzner W 2000 *Phys. Rev. Lett.* **85** 5162
- [31] Valenzuela B and Volzmediano M A H 2001 *Phys. Rev. B* **63** 153103
- [32] Furukawa N 1995 *J. Phys. Soc. Japan* **64** 2754
Furukawa N 1999 *Physics of Manganites* ed T A Kaplan and S D Mahanti (New York: Plenum) p 1
- [33] Perring T G, Aeppli G, Moritomo Y and Tokura Y 1997 *Phys. Rev. Lett.* **78** 3197
- [34] Kim K H, Uehara M, Hess C, Sharma P A and Cheong S-W 2000 *Phys. Rev. Lett.* **84** 2961
- [35] Babushkina N A, Taldenkov A N, Belova L M, Chistotina E A, Gorbenko O Yu, Kaul A R, Kugel K I and Khomskii D I 2000 *Phys. Rev. B* **62** R6081
- [36] Asamitsu A, Tomioka Y, Kuwahara H and Tokura Y 1997 *Nature* **388** 50
- [37] Moritomo Y, Kuwahara H, Tomioka Y and Tokura Y 1997 *Phys. Rev. B* **55** 7540
- [38] Kiryukhin V, Casa D, Hill J P, Keimer B, Vigliante A, Tomioka Y and Tokura Y 1997 *Nature* **386** 813
- [39] Miyano K, Tanaka T, Tomioka Y and Tokura Y 1997 *Phys. Rev. Lett.* **78** 4257
- [40] Dai P-C, Fernandez-Baca J A, Plummer E W, Tomioka Y and Tokura Y 2001 *Phys. Rev. B* **64** 224429
- [41] Yunoki S, Hu J, Malvezzi A L, Moreo A, Furukawa N and Dagotto E 1998 *Phys. Rev. Lett.* **80** 845
- [42] Arovas D P and Guinea F 1998 *Phys. Rev. B* **58** 9150
- [43] Burgy J, Mayr M, Martin-Mayor V, Moreo A and Dagotto E 2001 *Phys. Rev. Lett.* **87** 277202